ELSEVIER

Journal of Neuroscience Methods 87 (1999) 1–11

JOURNAL OF NEUROSCIENCE METHODS

Imaging neuronal calcium fluorescence at high spatio-temporal resolution

Marco Canepari, Fabio Mammano *

Laboratory of Biophysics and INFM Unit, International School for Advanced Studies, via Beirut 2-4, 34014 Trieste, Italy

Received 7 April 1998; received in revised form 8 July 1998; accepted 11 July 1998

Abstract

A rapid fluorescence imaging system was developed and utilised to investigate the time-course of intracellular calcium concentration ($[Ca^{2+}]_i$) gradients generated by action potentials in CA1-CA3 pyramidal cells within brain slices of the rat hippocampus. The system, which is based on a fast commercial CCD camera, can acquire hundreds of 128×128 pixel images in sequence, with minimal inter-frame interval of 2.5 ms (400 frames/s) and 12 bit/pixel accuracy. By synchronising patch clamp recordings with image capture, the timing of transmembrane potential variation, ionic Ca^{2+} current and Ca^{2+} diffusion were resolved at the limit of the relaxation time for the dye–Ca^{2+} binding reaction (approximately 5 ms at room temperature). Numerical simulations were used to relate measured fluorescence transients to the spatio-temporal distribution of intracellular Ca^{2+} gradients. The results obtained indicate that dye reaction–diffusion contributes critically to shaping intracellular ion gradients.

Keywords: CCD; Patch-clamp; Intracellular ion gradients; Reaction–diffusion modeling; Calcium green-1; Calcium crimson

1. Introduction

A pre-requisite for a quantitative analysis of neuronal function modulation by $[Ca^{2+}]_i$ is the possibility to measure ion concentration dynamics with sufficient spatio-temporal resolution. This paper describes a system for combining patch-clamp recording and fluorescence imaging at high frame rates using commercially available hardware. In order to evaluate system performance, we measured the time-course of $[Ca^{2+}]_i$ gradients generated by action potentials in hippocampal CA1-CA3 pyramidal cells within brain slices. Different Ca^{2+}-sensitive dyes, loaded into cells via patch-clamp pipettes, were evaluated in terms of stationary and time-dependent fluorescence signals. Image sequences were captured at 93–400 frames/s, revealing frequency dependent anisotropy of fluorescence increase in somas and proximal dendrites during trains of evoked action potentials. Synchronisation of image acquisition with voltage and current recordings permitted to characterise the timing of transmembrane potential variation, Ca^{2+} current and Ca^{2+} diffusion providing striking 2D visualizations of $[Ca^{2+}]_i$ gradients at the limit of the relaxation time for the dye–Ca^{2+} binding reaction. Numerical simulations on a model cell were used to gain a better understanding of the relationship between $[Ca^{2+}]_i$ and fluorescence measurements, as well as to provide indirect estimates for the endogenous buffering power in the soma. The results indicate that Ca^{2+} fluorescence signals must be included into realistic reaction–diffusion schemes in order to perform quantitative analysis of $[Ca^{2+}]_i$ gradients estimated from image sequences acquired at high frame-rates.

* Corresponding author. Tel.: +39 40 3787254; fax: +39 40 3787249; e-mail: mammano@sissa.it

0165-0270/99/$ - see front matter
PII: S0165-0270(98)00127-7

2. Methods

2.1. Fluorescence imaging

A modular upright microscope (MI 250, Newport-Microcontrole, Irvine, CA) was equipped with a $\times 63$ water-immersion objective (N.A. 0.90; Achroplan, Carl Zeiss, Jena, Germany) and an epi-fluorescence illuminator incorporating two dichroic filter-cubes (070103016 and 070103013, Nachet, Evry, France). These were used in combination with XF23 and XF41 excitation/emission interference filter sets (Omega Optical, Brattleboro, VT) for Calcium Green-1 and Calcium Crimson fluorescence, respectively. Excitation light from a 75-W stabilised Xenon arc source (Cairn Research, Faversham, Kent, UK) was coupled to the microscope via a liquid light guide gated by a rapid shutter (UniBlitz, Vincent Associates, Rochester, NY). Light was attenuated with a diaphragm to avoid phototoxicity and excessive bleaching. Fluorescence was measured using a fast CCD camera (CA-D1 128T, DALSA, Waterloo, Ontario, Canada) with 8 MHz readout rate and 12 bit/pixel precision. Each image was formed by an array of 128×128 pixels, corresponding to a spatial resolution of 0.78 μm/pixel. Distances in the specimen plane were calibrated once for all by placing a 10-μm pitch graticule under the objective.

2.2. Electrophysiology

Young Wistar rats (6- to 10-day-old) were decapitated under urethane anaesthesia (0.5 ml i.p. of a 10% solution). Brain hemispheres were rapidly isolated and placed in ice-cold standard solution containing (in mM): 126 NaCl, 3.5 KCl, 2 $CaCl_2$, 1.2 NaH_2PO_4, 1.3 $MgCl_2$, 25 $NaHCO_3$, 11 glucose, bubbled with 95% O_2 and 5% CO_2. Hippocampal slices of 200 μm thickness were prepared using a vibratome (Campden Instruments, Loughborough, UK) and immediately transferred to an incubation chamber containing the same solution at 32°C (pH 7.3). Slices were allowed to recover for at least 1 h before being moved to the recording chamber, in which they were superfused at 3 ml/min at room temperature (22–24°C). Electrical recordings were made from CA3 and CA1 pyramidal neurons in the slice using patch pipettes pulled from 2 mm o/d borosilicate glass. Pipettes had a resistance of 4–6 MΩ when filled with intracellular solution containing (in mM): 123 K-gluconate, 12 KCl, 4 $MgCl_2$, 10 HEPES, 4 Na_2ATP, 0.3 Na_2GTP, 10 phosphocreatine, adjusted to pH 7.2 with KOH. Impermeant potassium salts of calcium-sensitive fluorescent dyes Calcium Green-1 (470–500 nm excitation, 520–560 nm emission, dissociation constant $K_d = 190$ nM) and Calcium Crimson (540–580 nm excitation, 595–625 nm emission, $K_d = 185$ nM) were dissolved in intracellular solutions in the concentration range 35–150 μM and loaded into cells by establishing whole-cell recording conditions (Eilers et al., 1995) using a standard patch-clamp amplifier (EPC-7, List Medical Instruments). Patched cells had resting potentials of -62 ± 8 mV and were generally held at $V_h = -70$ mV. Input resistance near V_h was 182 ± 52 MΩ (mean ± S.D, $n = 54$). For voltage-clamp recordings, pipette capacitance, whole-cell capacitance and series resistance (50–60%) were compensated. Recordings were accepted for later analysis if the uncompensated series resistance did not exceed 20 MΩ. No correction for the junction potential between the bath and the pipette was made (approximately -11 mV; Neher, 1992). In some experiments, action-potential waveforms were constructed from current-clamp recordings obtained from a different cell in the same slice (Spruston et al., 1995), and played-back to the imaged neurone in voltage clamp. For these recordings, potassium channels were blocked by replacing K-gluconate and KCl with 135 CsCl in the intracellular solution whereas sodium channels were blocked by addition of 1 μM TTX (Affinity Research) to the superfusate.

2.3. Data acquisition and analysis

Electrical signals from the patch-clamp amplifier were filtered at 3 kHz and sampled at 10–20 kHz by a 12 bit laboratory interface (1401plus, Cambridge Electronic Design, Cambridge, UK) using customised control software. The frame-enable signal from the CCD camera was also sampled, allowing for off-line determination of current, voltage and image acquisition timing. The control signals required to trigger the optical section of the set-up were generated by the same software and interface. Image sequences were acquired at 93–400 frames/s, digitised at 12 bit/pixel and stored in real time to the RAM of a Pentium PC using a high-performance frame-grabber (IC-PCI/AM-DIG16, Imaging Technology, Bedford, MA) controlled by macros written in Optimas 5.0 language (Optimas Corporation, Bothell, WA). The camera operated in an efficient frame-transfer mode, whereby pixel data were shifted from the light-exposed to the masked region of the CCD sensor in less than 4% of the inter-frame interval. This avoided image blurring and maximised photocharge integration time. Accepted images were saved on a UW-SCSI hard drive and analysed using routines developed from Matlab 5.1 Image Processing Toolbox (The Mathworks Inc., Natick, MA). For each image pixel, fluorescence signals were computed as ratios:

$$\frac{\Delta F(t)}{F(0)} = \frac{F(t) - F(0)}{F(0)} \quad (1)$$

In this expression, t is time, $F(t)$ is fluorescence following a stimulus that causes calcium elevation

Table 1
Parameters used for numerical computations

Symbol	Definition	Value	Comment
Geometry			
r_o	Cell radius	7.5 μm	Used by Nowycky and Pinter (1993)
dr	Shell thickness	0.25 μm	Intracellular space discretized in 30 concentric shells
Calcium			
I_{Ca}	Ca current	400 pA	Peak value; waveform as shown in Fig. 5A
$[Ca^{2+}]_i$	Initial Ca concentration	0.05 μM	Helmchen et al. (1996)
D_{Ca}	Diffusion constant for free calcium in cytoplasm	220 $\mu m^2/s$	Allbritton et al. (1992)
Fixed buffer			
$[B_s]$	Total concentration	530 μM	Similar to Nowycky and Pinter (1993)
$K_D^{B_s}$	Dissociation constant	3800 μM	Concentration and affinity selected so that $\kappa \approx 120$.
$K_{on}^{B_s}$	Forward binding rate	570 μM/s	Equal to dye's, see also Klingauf and Neher (1997)
Mobile buffer (dye)			
$[B_m]$	Total concentration	75 μM	Used in most experiments
$K_D^{B_m}$	Dissociation constant	0.190 μM	CG-1, Molecular Probes estimate
$K_{on}^{B_m}$	Forward binding rate	570 μM/s	Eberhard and Erne (1991)
D_{B_m}	Diffusion constant	200 $\mu m^2/s$	Used by Nowycky and Pinter (1993)

within the cell and $F(0)$ is pre-stimulus fluorescence computed by averaging 10–20 images. Both $F(t)$ and $F(0)$ were corrected for mean auto-fluorescence computed from a 20×20 pixel rectangle devoid of obvious cellular structures. Ratio magnitude was encoded by 8 bit pseudo-color look-up tables to produce false-colour images. The local ratio computation in Eq. (1) is expected to provide correction for time-independent non-uniformity in optical path-length and dye concentration (Neher and Augustine, 1992). This was kept as constant as possible during image acquisition by waiting until dye dialysis had produced stable $F(0)$ values (15–20 min with input resistance ≤ 15 MΩ). Excitation intensity was adjusted to produce photo-bleaching rates $\leq 0.5\%/s$ during tens of 1-s long illumination periods. Where indicated, a three-point zero-phase digital filter (Oppenheim and Shaffer, 1989) and a 3×3 two-dimensional median filter (Lim, 1990) were applied to fluorescence traces and images, respectively.

2.4. Diffusion–reaction modelling

To model the dynamics of Ca^{2+} entering the soma of pyramidal cells, the computational scheme proposed by Nowycky and Pinter (1993) was adopted. Briefly, $[Ca^{2+}]_i$ was evaluated as a function of time t and radial distance r in a spherical cell following uniform Ca^{2+} entry across the outer membrane. The sphere volume was subdivided into discrete shells and diffusion–reaction of Ca^{2+} with a mobile exogenous buffer (dye) of absolute concentration $[B_m]$ and an immobile endogenous buffer of concentration $[B_s]$ was described in the following manner:

$$\begin{aligned}\frac{\partial[Ca^{2+}]_i}{\partial t} &= \int_0^{r_0} \delta(r - r_o)\frac{I_{Ca}}{2FV_o}\,dr \\ &+ D_{Ca}\left(\frac{\partial^2[Ca^{2+}]_i}{\partial r^2} + \frac{2}{r}\frac{\partial[Ca^{2+}]_i}{\partial r}\right) \\ &- K_{on}^{B_m}[B_m][Ca^{2+}]_i + K_{off}^{B_m}[B_mCa] \\ &- K_{on}^{B_s}[B_s][Ca^{2+}]_i + K_{off}^{B_s}[B_sCa]\end{aligned} \quad (2)$$

Here D_{Ca} is Ca^{2+} diffusion coefficient in the cytoplasm, K_{on}^X is the association rate constant of calcium binding to buffer X (B_m or B_s), K_{off}^X is the dissociation rate of calcium from the (X Ca) complex[1], I_{Ca} is transmembrane calcium current, F is Faraday's constant, V_o is the volume of the shell just below the membrane (Yamada et al., 1989), δ is Dirac's delta and r_o the cell radius. The first line of the equation's right hand side (r.h.s.) represents a transmembrane source of calcium, the second radial diffusion, the third binding of calcium to dye and the fourth binding of calcium to the endogenous buffer. The reaction–diffusion of B_m as well as of the (B_m Ca) complex was described by two analogous equations without source terms. Finally, two more equations, missing both radial diffusion and source, were used to compute the changes of $[B_s]$ and $[B_s\ Ca]$. Table 1 lists the parameters used for numerical computations.

[1] The dissociation constant K_D^X for the reaction $X + Ca^{2+} \leftrightarrow$(X Ca) equals K_{off}^X/K_{on}^X

3. Results

3.1. Imaging rapid calcium concentration gradients

Video microscopy exploiting IR asymmetric illumination contrast (Kachar, 1985; Mammano et al., 1995) was used to image CA3 and CA1 hippocampal pyramidal neurones in rat brain slices. Identified cells having proximal apical dendrites in the horizontal plane of focus were patch-clamped under direct visual control with pipettes containing cell-impermeant Calcium Green-1 (75 μM). The maximal changes in fluorescence observed in the present set of experiments amounted to less than 30% $\Delta F(t)/F(0)$ and were typically less than 10%, whereas test applications of 25 mM K^+ and 150 μM *N*-methyl-D-aspartate to the bath caused $\Delta F(t)/F(0)$ to increase by more that 100%, indicating that the dye was not binding Ca^{2+} near saturation. In other control experiments, $\Delta F(t)/F(0)$ signals following an action-potential were reduced below detection threshold by adding to the superfusate broad spectrum blockers of voltage activated calcium channels Ni^{2+} (50 μM) and Cd^{2+} (200 μM). In contrast, contribution to Ca^{2+} influx from NMDA receptors (Garaschuk et al., 1996) was probably too small to be measured under the present recording conditions, as block by extracellular (+)-3-(carboxypiperazin-4-yl)-propyl-1-phosphonic acid (CPP, 20 μM; a gift of Dr Herrling, Novartis, Basel) did not produce appreciable changes in $\Delta F(t)/F(0)$.

The peak amplitude of $\Delta F(t)/F(0)$ transients following a single action potential was a monotonically decreasing function of Calcium Green-1 concentration in the range 35–150 μm (Fig. 1A) (Borst et al., 1995; Helmchen et al., 1996, 1997). At 75 μM, resting fluorescence $F(0)$ was twofold higher for Calcium Crimson than for Calcium Green-1 (Fig. 1C, solid bars). This is probably due to a combination of different dye affinities and compartmentalisation, as well as sensor quantum efficiency (Fig. 1B) at the different wavelengths used. Peak values of $\Delta F(t)/F(0)$ transients for Calcium Green-1 and Calcium Crimson differed by a factor of 3 or more (Fig. 1C, empty bars), which is only partially accounted for by the two-fold difference in denominator values. Fluorescence signals following single action potentials were measured from cell somas with typical S/N ≥ 6 for Calcium Green-1 and ≥ 4 for Calcium Crimson (single-pixel values for data collected at 200 frames/s using dye concentration of 75 μm in the pipette).

Fig. 2 shows one representative data set from experiments in which Ca^{2+}-dependent changes in dye fluorescence were measured at full-frame resolution (128 × 128 pixels) with a temporal resolution of 10.8 ms, as described in Section 2, from large CA3 pyramidal cells. Successive action potentials elicited by somatic injection of current pulses produced distinguishable contributions to Ca^{2+} entry. Individual contributions were resolved down to about 20 ms inter-spike intervals at the cell periphery (Fig. 2B, green trace). By contrast,

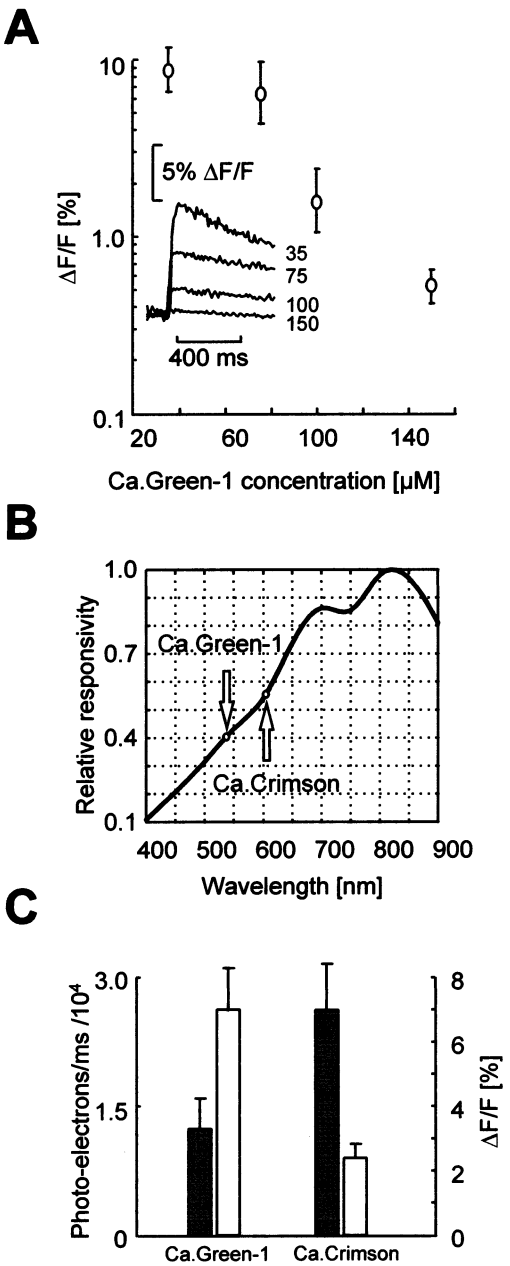

Fig. 1. Dye response characterization. (A) Fluorescence peak response of Calcium Green-1 to a single action-potential, plotted against dye concentration. Inset: four unfiltered sample responses from different cells at shown dye concentrations (μM). (B) Relative spectral responsivity of the DALSA CA-D1 CCD sensor, adapted from camera data sheet. Arrows correspond to dye maximal emission wavelength (Kao, 1994). (C) Mean neuronal stationary (pre-stimulus) fluorescence measured at the single pixel level (solid bars, left axis) and single action-potential evoked fluorescence peak response (hollow bars, right axis) for Calcium Green-1 and Calcium Crimson. Dyes were loaded into CA1-CA3 pyramidal cells at 75 μM pipette concentration. Data in (A) and (C) are mean ± S.D. ($n = 5$ cells).

$\Delta F(t)/F(0)$ increased in a markedly more continuous fashion near the cell center (Fig. 2B, red trace). Thus substantial $[Ca^{2+}]_i$ gradients developed rapidly within the cell cytoplasm, with instantaneous magnitude depending strongly on the cell firing frequency. These recordings were also characterised by conspicuous delays between fluorescence and voltage peaking. As shown in Fig. 2C (first frame), no fluorescence changes could be detected during the course of an action potential. The delayed $\Delta F(t)/F(0)$ signal reached a maximum near the cell boundary only 19.8 ± 7.3 ms ($n = 6$ cells) after the peak of an action potential, generating a characteristic annular pattern of fluorescence (Fig. 2C, second and third frame). The annular front relaxed towards the cell centre in 178 ± 45 ms as diffusion caused progressive re-equilibration of cytoplasmic Ca^{2+} (Fig. 2D and 2E). Somatic fluorescence returned to baseline levels a few seconds after the last action potential (time constant 1.2 ± 0.3 s, as measured by mono-exponential fits following a single action-potential, with 75 μM Calcium Green-1 in the pipette), as a consequence of cell buffering and extrusion.

3.2. Timing of calcium entry

It was suggested a long time ago that, in the squid axon, most of the Ca^{2+} enters during the re-polarisation phase of the action potential (Llinas et al., 1981). Thus, a series of experiments was undertaken using faster frame rates (5.4-ms inter-frame interval) commanding membrane potential to follow the waveform of simulated action potentials (Doerr et al., 1989) (Fig. 3A, top trace) after establishing pharmacological conditions that permitted the selective detection of Ca^{2+} currents (see Section 2).

The fast inward currents elicited under these conditions (Fig. 3A, bottom trace) were reduced by more than 90% by superfusion with nominally zero extracellular Ca^{2+}. The simplest explanation is that simulated action potentials elicited essentially Ca^{2+} tail currents generated by the sudden increase in driving force following membrane re-polarisation, whereas little or no current flowed during the brief depolarisation phase even though the channels were opened (Johnston and Wu, 1995). Current integration revealed that Ca^{2+} influx following an action potential was rather large ($5.7 \pm 2.1 \times 10^{-17}$ mol, $n = 3$ cells). Similar results have been obtained in DRG cells from chick embryos (McCobb and Beam, 1991) as well as in a calyx type synapse in the rat medial nucleus of the trapezoid body (Borst and Sakmann, 1996). Detectable $\Delta F(t)/F(0)$ signals were produced only after the Ca^{2+} current had peaked, approximately 5 ms after the maximum of the simulated action potential. The relaxation time of the dye–Ca^{2+} binding reaction (Kao and Tsien, 1988) further delayed the rise of the $\Delta F(t)/F(0)$ signal near the cell boundary by several ms. However, it should be pointed out that a substantial fraction of the whole-cell Ca^{2+} current originated likely from unclamped regions of the membrane which did not experience the commanded action-potential waveform. Therefore, the timing of the currents reported here is probably not entirely reliable and these should be understood as attenuated and distorted versions of the real Ca^{2+} currents flowing during a natural action potential.

3.3. Frequency-dependent calcium responses

Action potentials are known to actively invade the apical dendritic tree of CA1 pyramidal neurons (Jaffe et al., 1992; Andreasen and Lambert, 1995; Stuart et al., 1997) in a frequency-dependent manner (Callaway and Ross, 1995; Tsubokawa and Ross, 1996). In this final set of experiments, repetitive action potentials were elicited in CA1 neurones by trains of brief somatic current pulses. For stimulation frequencies up to 40 Hz, one action potential was usually evoked by each pulse.

In general, only a fraction of the apical dendrite (up to 90–100 μm from the soma) was clearly distinguishable with sufficient S/N. However, the intensity of fluorescence signals was different even in such relatively limited portions of the imaged cells, as shown in Fig. 4. In particular $\Delta F(t)/F(0)$ relative maxima formed 40–60 μm from the soma, irrespective of action potential frequency. In the soma, $\Delta F(t)/F(0)$ increased linearly with the number of action potentials, whereas in the proximal dendrite (up to 60 μm from the soma) $\Delta F(t)/F(0)$ increment was comparatively attenuated. Finally, beyond the first noticeable dendritic branching, fluorescence failed to rise after the first few action potentials in a train. Differences in these three distinct patterns of $\Delta F(t)/F(0)$ dynamics were particularly evident at the highest stimulation frequency used (40 Hz) in accord with previous experimental and theoretical investigations (Jaffe et al., 1994). A likely explanation for the compartmentalisation of the $\Delta F(t)/F(0)$ rise is the anisotropic distribution of Ca^{2+} channels (Christie et al., 1995) whereas failure of action potential invasion, possibly due to the presence of transient A-type K^+ channels in the dendrites of CA1 pyramidal neurones (Hoffman et al., 1997), may account for the $\Delta F(t)/F(0)$ behaviour at dendritic branch points (Spruston et al., 1995).

3.4. Modelling somatic $[Ca^{2+}]_i$ dynamics

The results in Figs. 2–4 indicate that Ca^{2+} imaging can be performed in brain slices with high spatial resolution under conditions whereby the ultimate tem-

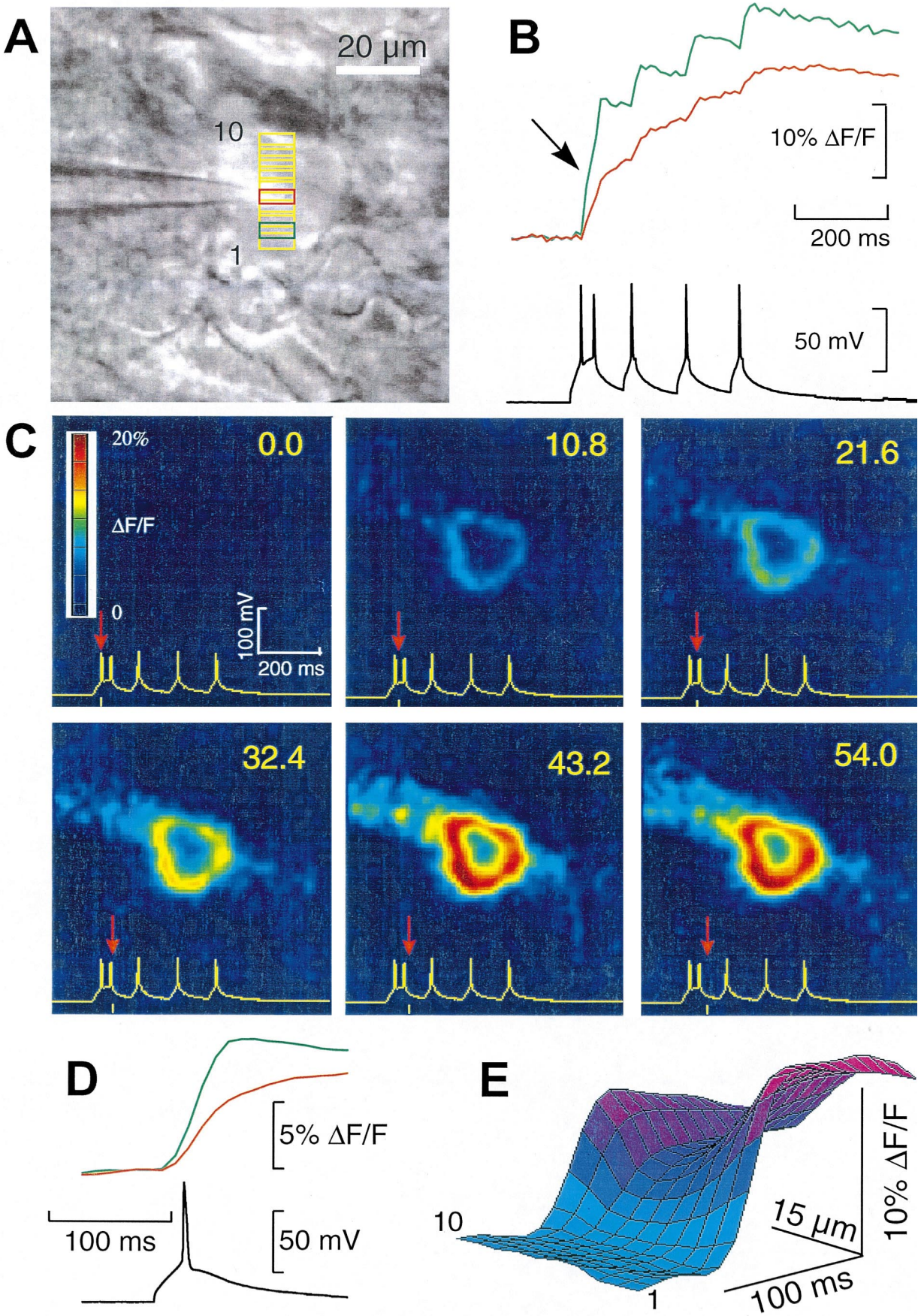
A
20 µm
10
1
B
10% ΔF/F
200 ms
50 mV
C
20%
ΔF/F
0
100 mV
200 ms
0.0
10.8
21.6
32.4
43.2
54.0
D
5% ΔF/F
100 ms
50 mV
E
10
1
15 µm
100 ms
10% ΔF/F

Fig. 2.

poral limitation is set by the kinetic properties of the fluorescent indicator used. Specifically, the time-course of fluorescence transients at stimulus onset was influenced by dye relaxation time τ, which is given by the expression (Kao and Tsien, 1988):

$$\frac{1}{\tau} = K_{on}[Ca^{2+}]_i + K_{off} \quad (3)$$

K_{on} and K_{off} are, respectively, thermodynamic association and dissociation constants for the binding of calcium to dye. Following an action potential, $[Ca^{2+}]_i$ is likely to rise locally to ≈ 300 nM (Helmchen et al., 1996). Thus, using published figures for the rate constants (Eberhard and Erne, 1991; see Table 2), values for τ of ≈ 3.2 and ≈ 2.5 ms can be estimated, at room temperature, for Calcium Green-1 and Calcium Crimson, respectively.

Fluorescent dyes are not expected to track accurately $[Ca^{2+}]_i$ changes that take place on a time scale faster than $3–4\tau \approx 10$ ms (Kao and Tsien, 1988), in good agreement with the results shown in Figs. 2 and 3. In order to achieve a better understanding of $[Ca^{2+}]_i$ transients in the soma of pyramidal cells, a simple model of reaction–diffusion in a spherical cell was utilised (Sala and Hernández-Cruz, 1990). The model included Ca^{2+} and a fast high-affinity mobile buffer (dye) of concentration $[B_m]$ as diffusing species. Binding of Ca^{2+} to dye occurred in the presence of a low affinity immobile buffer of concentration $[B_s]$, which competed for Ca^{2+}. To keep the model as simple as possible, Ca^{2+} leakage and extrusion were not included. Model parameters were selected from the experimental and theoretical literature (Table 1), with the exception of the dissociation constant $K_D^{B_s}$ of $[B_s]$ which was adjusted by trial-and-error to produce responses in reasonable agreement with experimental data.

Fig. 5 shows model responses to brief injection of a Ca^{2+} current (Fig. 5A) peaking ≈ 5 ms after the maximum of the action potential, taken as $t = 0$, and decaying in ≈ 10 ms (see Fig. 3A). The largest current value, 400 pA, was selected in agreement with experimental results, considering that about 20% of the total current entered from the soma. The time course of $[Ca^{2+}]_i$ at different depths below the cells surface (0.25, 1.5, 3.0, 4.5 and 6.0 μm) is shown in Fig. 5B. In the outermost shell $[Ca^{2+}]_i$ reached peak values ≈ 300 nM a few ms after the current peak, but rose at a considerably slower rate progressing towards the cell centre. As clearly evident in Fig. 5C, the distribution of the dye–calcium complex at the same depths represents a delayed and distorted version of $[Ca^{2+}]_i$. To compare model predictions to experimental results, contribution from out-of-focus fluorescence (Hiraoka et al., 1990) was taken into account by adding a weighted average of signals from peripheral shells to inner shells (Fig. 5D). Finally, model output was averaged over 5-ms intervals to simulate photo-charge integration by the CCD sensor (Fig. 5E, dashed lines). The combination of model values for total $[B_s]$ and $K_D^{B_s}$ corresponded to an incremental Ca^{2+}-binding ratio (Neher and Augustine, 1992)

$$\kappa = \frac{\Delta[B_s Ca]}{\Delta[Ca^{2+}]_i} = \frac{[B_s]K_D^{B_s}}{([Ca^{2+}]_{rest} + K_D^{B_s})([Ca^{2+}]_{peak} + K_D^{B_s})} \quad (4)$$

of about 120 (mean value, averaged over all discrete shells in which the intracellular space was subdivided). For comparison, values of κ in the range 64–186 were estimated experimentally in the proximal apical dendrites of hippocampal CA1 neurones (Helmchen et al., 1996).

4. Discussion

This work describes a rapid imaging system used to investigate the time-course of $[Ca^{2+}]_i$ gradients generated by action potentials in pyramidal cells within brain slices of the rat hippocampus. Intracellular

Fig. 2. Development of fast $[Ca^{2+}]_i$ gradients. (A) Infra-red transmitted-light image of a CA3 pyramidal neuron in a 200-μm thick brain slice from rat hippocampus, with a superimposed array of ten partially overlapping regions of interest (ROIs). A patch pipette, used to load the cell with 75 μM Calcium Green-1, is seen entering from left. A short dendritic segment, proceeding at approximately 45° from the cell soma towards the top-left image corner, is also visible. (B) Simultaneous recordings of transmembrane voltage (bottom trace) and unfiltered means of fluorescence change from the red (middle trace) and green (upper trace) ROIs in (A). Potential was measured in current-clamp in response to somatic injection of four 30-ms 200-pA pulses. The first pulse evoked two action potentials in rapid succession (26-ms inter-spike interval). Contribution to calcium entry from each of these two action potentials is clearly identifiable as a slope change in the $\Delta F(t)/F(0)$ rise time course measured at the cell boundary (arrow). Inter-frame interval was 10.8 ms (93 frames/s). (C) Six selected false-color images from the sequence collected during the recordings in (B). The color scale-bar is reproduced on the first image. Time in ms after the first action potential in (B) is displayed in the top right corner of each image. Voltage trace from (B) is also shown for clarity at frame bottom as a solid yellow line and the time of frame capture is marked by a red downward arrow. (D) Bottom: single action potential evoked by a 30-ms 200-pA somatic current-pulse injection in the same cell. Top: corresponding fluorescence changes measured from the red and green ROIs in (A). ROI and trace colors are matched. (E) Space-time 3D plot: receding axis is distance along the cell profile, from ROI 1 to 10, abscissa is time, surface height gives local fluorescence change (also encoded as surface color).

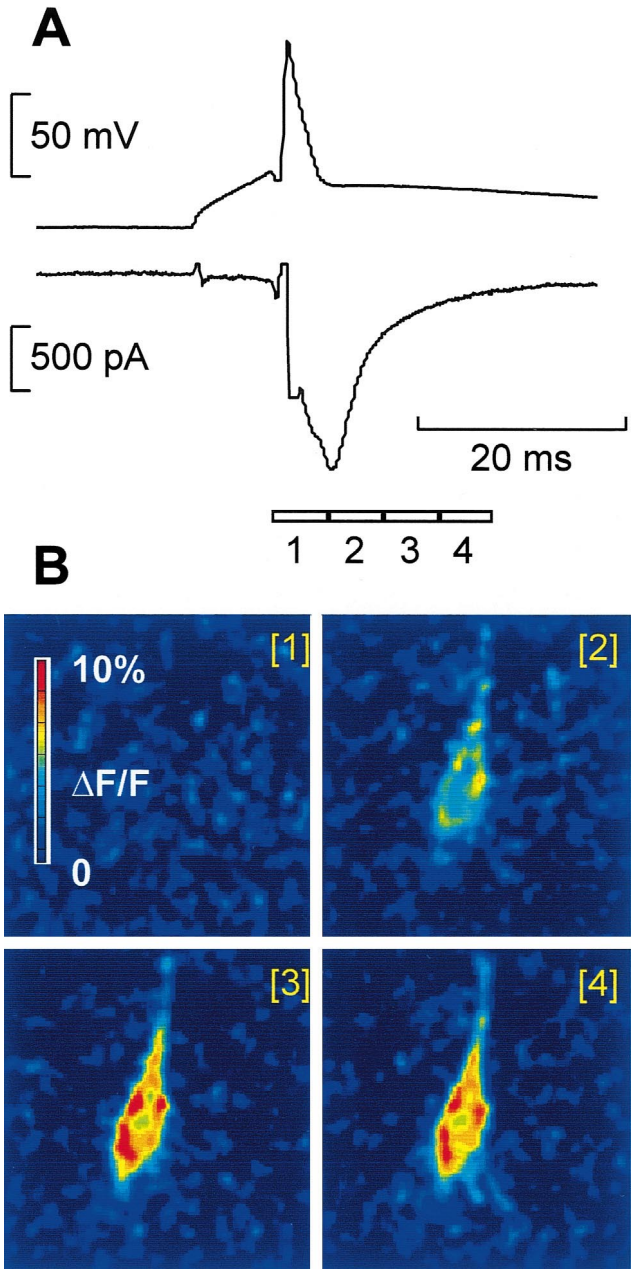

Fig. 3. Calcium entry and calcium current. (A) Patch-clamp recordings from a CA1 pyramidal neuron loaded with 75 μM Calcium Green-1 in a CsCl-based intracellular solution and in the presence of 1 μM extracellular TTX. Top: simulated action-potential applied under voltage-clamp. The voltage wave-form was obtained from a different cell in the same slice under current-clamp using a K-gluconate based intracellular solution (and no TTX). Bottom: calcium current trace representing the difference between the recordings obtained in 2 mM and nominally zero extracellular calcium. (B) Four false-color consecutive images taken at 5.4 ms intervals during the voltage-clamp recording in (A). Photo-charge integration intervals are marked by boxes at the bottom of (A); box separation lines indicate the short frame-shift periods during which CCD integration was disabled (see Section 2).

Ca^{2+} was visualised by loading cells with fluorescent-dyes selective for this ion and measuring fluorescent transients using a fast CCD camera.

4.1. Imaging Ca^{2+} transients at high frame-rate

Fast Ca^{2+} imaging (i.e. faster than standard video-rate) of $[Ca^{2+}]_i$ gradients has been performed either with confocal microscopy operating in the line-scan mode (Hernandez-Cruz et al., 1990), or with cooled CCD devices (Lasser-Ross et al., 1991). In this present work, a substantial effort was devoted to achieve simultaneously high spatial and temporal resolution of fluorescence signal detection. The system utilised was capable of capturing hundreds of images in sequence with minimal 2.5 ms inter-frame interval at full-frame resolution (128 × 128 pixels) with 12 bit/pixel precision. Data presented in this paper was acquired at inter-frame intervals between 10.8 and 5.0 ms. Because of the short integration times used, photon shot-noise N_{Ph}[2] proved to be the dominant factor in these experiments, which made CCD cooling unnecessary above about 90 frames/s. The relative performances of two single-wavelength dyes, Calcium Green-1 and Calcium Crimson, were evaluated in terms of stationary and time-dependent fluorescence signals. Despite the smaller $\Delta F(t)$ signals produced, Calcium Crimson allowed fluorescence transient measurements at higher frame rates than Calcium Green-1 whose lower resting fluorescence (Fig. 1) made it difficult to estimate reliably $F(0)$ above 200 frames/s.

4.2. Dye kinetics

At the high rates utilised, the limiting factor proved to be the dye relaxation time τ (Eq. (3)) so that frequencies higher than 200 frames/s would seem unnecessary for measuring $[Ca^{2+}]_i$ transients at room temperature. In fact, $\Delta F(t)/F(0)$ responses elicited by single action-potentials were detected at the maximum camera rate of 400 frames/s without appreciable differences (data not shown). However, given the relatively steep dependence on temperature of the $\Delta F(t)/F(0)$ rise time course (Markram et al., 1995), faster acquisition rates are probably required around physiological temperature.

4.3. Interpretation of fluorescence signal gradients

High frame-rate imaging permitted the 2D visualisation of the substantial $[Ca^{2+}]_i$ gradients that developed rapidly within the cell cytoplasm following action potentials (Figs. 2C and 3B), with local and instantaneous magnitude depending strongly on the cell firing fre-

[2] The overall noise associated with the acquisition of an image by a CCD device is $N_T = (N_R^2 + N_D^2 + N_{Ph}^2)^{1/2}$. Here N_R and N_D are the readout noise and the dark-charge noise of the CCD, respectively, whereas N_{Ph} is the photon shot-noise associated with the fluorescence signal.

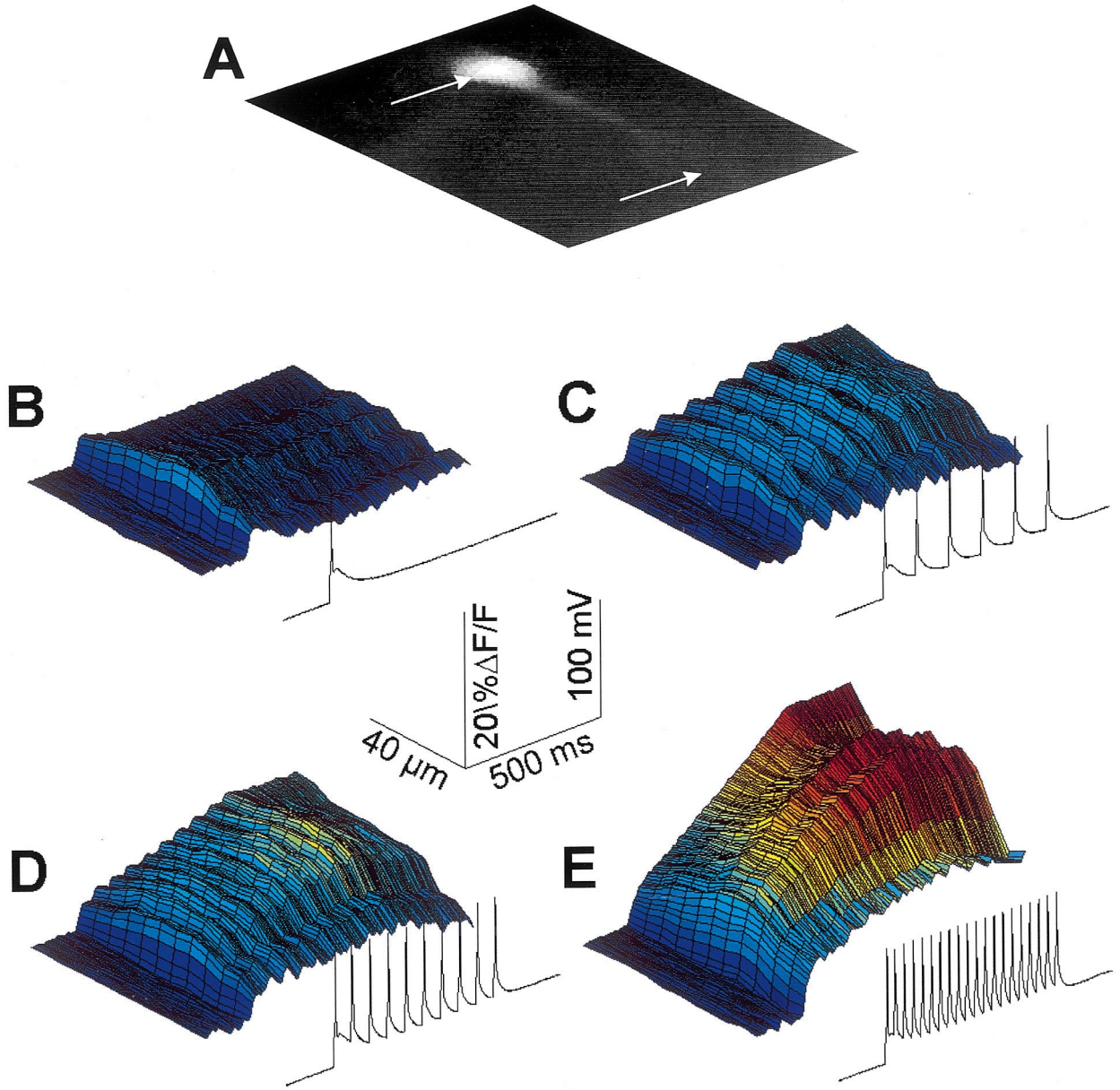

Fig. 4. Time-resolved spatial distribution of calcium entry during evoked action potential activity. (A) Fluorescence image of a CA1 hippocampal pyramidal neuron loaded with 75 μM Calcium Crimson. (B) Solid line: membrane potential versus time. A single action potential was evoked by intra-somatic current pulse injection (450 pA, 10 ms) via the loading pipette in whole-cell current-clamp. Space–time 3D plot: receding axis is distance along the cell profile, measured between the positions marked by arrows in (A); abscissa is time (same as voltage record); surface height represents mean relative fluorescence changes (also encoded as surface color) measured from 1 ROI partially covering the soma width and 11 partially overlapping ROIs stretched across the proximal dendrite (ROIs not shown). Data refers to a sequence of 180 frames captured at 5.0-ms inter-frame interval. (C) Same as (B), for repetitive current pulse injection (450 pA, 10 ms) at inter-pulse intervals of 100 ms. (D) 50 ms. (E) 25 ms.

quency (Figs. 2B and 4). However, it is important to realise that fast imaging of Ca^{2+} poses also a number of problems when trying to derive a quantitative estimate $[Ca^{2+}]_i$ from $\Delta F(t)/F(0)$, that is to say from the concentration of intracellular dye-bound calcium $[B_m Ca^{2+}]_i$. The common assumption is that ion and dye are locally in equilibrium so that $[Ca^{2+}]_i$ can be derived from the mass-action law (Thomas and Delaville, 1988). This is reasonable when $[B_m Ca^{2+}]_i$ gradients are imaged by integrating fluorescence signals over intervals significantly longer than τ (Williams et al., 1985; Neher and Augustine, 1992), but not for the short exposure times used in the present experiments. Numerical simulations on an extremely simplified spherical cell model showed that diffusion patterns for $[Ca^{2+}]_i$ can differ substantially from those reported by

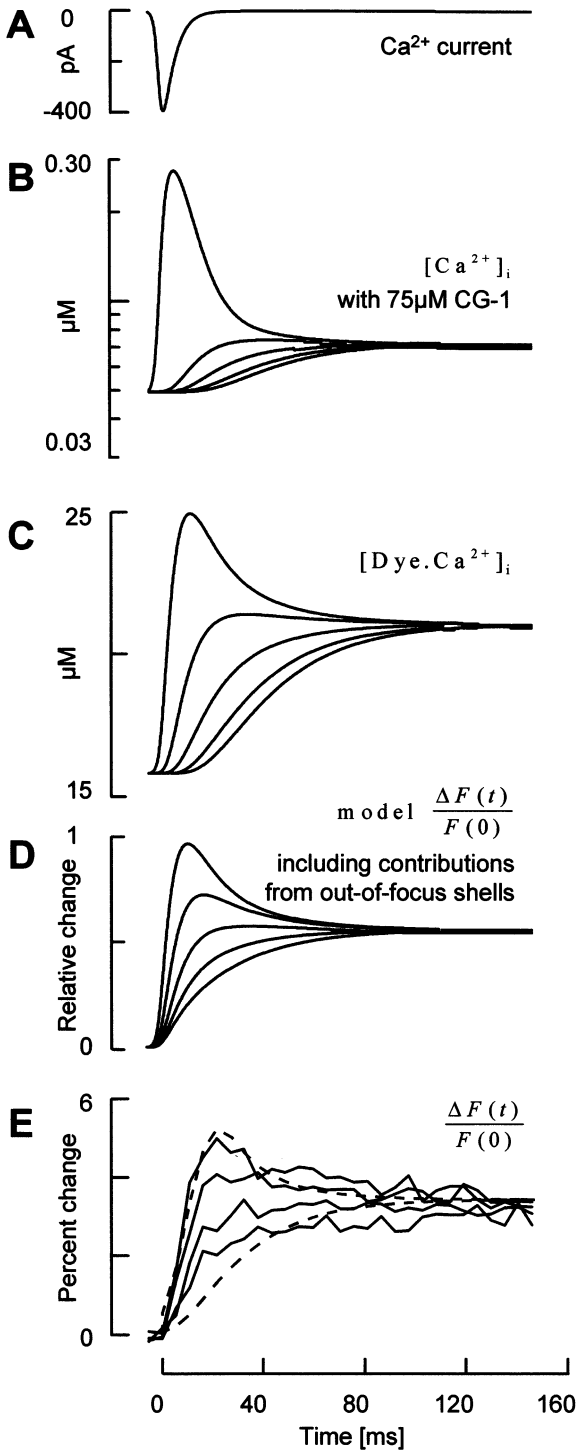

Fig. 5. Modeling calcium entry into the soma of pyramidal cells. (A) Time waveform of the Ca^{2+} current ICa used in the source term of Eq.2. (B) $[Ca^{2+}]_i$ time course at various depths within the cell: 0.25, 1.5, 3.0, 4.5 and 6 μm from the surface, top to bottom. Notice logarithmic scale on ordinates. (C) Time course of the calcium–dye complex concentration $[BmCa^{2+}]_i$ at the same depths as in (B). Notice linear scale on ordinates. (D) Relative change in model fluorescence signals associated with $[B_mCa^{2+}]_i$ distribution. Signals from inner shells included a weighted average of out-of-focus contributions from more peripheral shells. (E) Solid lines: sample fluorescence responses following a single action potentials in a CA3 pyramidal cell loaded with 75 μm Calcium Green-1. Unfiltered traces were generated by averaging real fluorescence images captured at 5.4-ms intervals from 2×2 μm contiguous regions covering the space from surface to center of the cell. Dashed lines represent a scaled version of the uppermost and lowermost trace in (D), averaged over 5.4 ms periods to simulate CCD photo-charge integration during image acquisition.

Table 2
Dye rate constants[a]

T (°C)	Calcium Green		Calcium Crimson	
	K_{off} (s)	K_{on} (μM/s)	K_{off} (s)	K_{on} (μM/s)
20.5	139	570	187	710

[a] From Eberhard and Erne (1991), Table 4.

$\Delta F(t)/F(0)$ (compare Fig. 5B and D). For fixed incremental Ca^{2+}-binding ratio around 120, $[B_mCa^{2+}]_i$ distributions agreed with measured fluorescence gradients only for $D_{Bm} \approx D_{Ca}$, indicating that the presence of a rapidly diffusing dye may substantially alter the time course of the 'unperturbed' somatic $[Ca^{2+}]_i$ gradients. Therefore, as evidenced also by other experiments conducted on the same as well as on different preparations, calcium transients depend strongly on the type and concentration of the dye used (Helmchen et al., 1996; Regehr and Atluri, 1995; Helmchen et al., 1997). The problem cannot be solved simply by lowering the dye concentration as rapid $[Ca^{2+}]_i$ elevations would just saturate the dye faster, particularly near the cell membrane, producing a non-linear fluorescence response. For these reasons, $\Delta F(t)/F(0)$ should be understood to represent, at best, a low-pass filtered version of the free Ca^{2+} transients (Nowycky and Pinter, 1993). It appears that the challenge for the future would be to perform quantitative analysis of rapid $[Ca^{2+}]_i$ gradients using fluorescence data in the context of realistic reaction–diffusion schemes, taking into account the details of cell geometry and channel distribution (Schaff et al., 1997).

Acknowledgements

This work was supported by SISSA Grant N.2101 'Nuove Iniziative di Sviluppo'. We thank Professors J. Ashmore (UCL, London), E. Cherubini (SISSA, Trieste), M. Hausser (UCL, London), B. Kachar (NIH, Bethesda), E. Neher (MPI, Goettingen), R. Nobili (University of Padova), V. Torre (SISSA, Trieste) and Drs G. Capello and I. Razaq (ICTP, Trieste) for critical comments on the manuscript. FM was supported by a Fellowship from the International Centre for Genetic Engineering and Biotechnology (ICGEB), Trieste.

References

Allbritton NL, Meyer T, Stryer L. Range of messenger action of calcium ion and inositol 1,4,5-triphosphate. Science 1992;258:1812–5.

Andreasen M, Lambert JDC. Regenerative properties of pyramidal cell dendrites in area CA1 of the rat hippocampus. J Physiol 1995;483:421–41.

Borst JGG, Sakmann B. Calcium influx and transmitter release in a fast CNS synapse. Nature 1996;383:431–4.

Borst JGG, Helmchen F, Sakmann B. Presynaptic and postsynaptic whole-cell recordings in the medial nucleus of the trapezoid body of the rat. J Physiol 1995;489:825–40.

Callaway JC, Ross WN. Frequency-dependent propagation of sodium action-potentials in dendrites of hippocampal CA1 pyramidal neurons. J Neurophysiol 1995;74:1395–403.

Christie BR, Eliot LS, Ito K, Miyakawa H, Johnston D. Different Ca^{2+} channels in soma and dendrites of hippocampal pyramidal neurons mediate spike-induced Ca^{2+} influx. J Neurophysiol 1995;73:2553–7.

Doerr T, Denger R, Trautwein W. Calcium currents in single SA nodal cells of the rabbit heart studied with action potential clamp. Pflüger's Arch 1989;413:599–603.

Eberhard M, Erne P. Calcium binding to fluorescent calcium indicators: Calcium Green, Calcium Orange and Calcium Crimson. Biochem Biophys Res Commun 1991;180:209–15.

Eilers J, Schneggenburger R, Konnerth A. Patch clamp and calcium imaging in brain slices. In: Sakmann B, Neher E, editors. Single Channel Recording. New York: Plenum Press, 1995:213–29.

Garaschuk O, Schneggenburger R, Schirra C, Tempia F, Konnert A. Fractional Ca^{2+} currents through somatic and dendritic glutamate-receptor channels of rat hippocampal CA1 pyramidal neurons. J Physiol 1996;491:757–72.

Helmchen F, Imoto K, Sakmann B. Ca^{2+} buffering and action potential-evoked Ca^{2+} signaling in dendrites of pyramidal neurons. Biophys J 1996;70:1069–81.

Helmchen F, Borst JGG, Sakmann B. Calcium dynamics associated with a single action potential in a CNS presynaptic terminal. Biophys J 1997;72:1458–71.

Hernandez-Cruz A, Sala F, Adams PR. Subcellular calcium transients visualized by confocal microscopy in a voltage-clamped vertebrate neuron. Science 1990;247:858–62.

Hiraoka Y, Sedat JW, Agard DA. Determination of three-dimensional imaging properties of a light microscope system. Biophys J 1990;57:325–33.

Hoffman DA, Magee JC, Colbert CM, Johnston D. K^+ channel regulation of signal propagation in dendrites of hippocampal pyramidal neurons. Nature 1997;387:869–75.

Jaffe DB, Johnston D, Lasser-Ross N, Lisman JE, Miyakawa H, Ross WN. The spread of Na^+ spikes determines the pattern of dendritic Ca^{2+} entry into hippocampal neurons. Nature 1992;357:244–6.

Jaffe DB, Ross WN, Lisman JE, Lasser-Ross N, Miyakawa H, Johnston D. A model for dendritic Ca^{2+} accumulation in hippocampal pyramidal neurons based on fluorescence imaging measurements. J Neurophysiol 1994;71:1065–77.

Johnston D, Wu SM. Foundations of Cellular Neurophysiology. Cambridge, MA: MIT Press, 1995:334–8.

Kachar B. Asymmetric illumination contrast: a method of image formation for video light microscopy. Science 1985;227:766–8.

Kao JP. Practical aspects of measuring $[Ca^{2+}]$ with fluorescent indicators. In: Nuccitelli R, editor. A Practical Guide to the Study of Calcium in Living Cells. San Diego: Academic Press, 1995:155–81.

Kao JP, Tsien RY. Ca^{2+} binding kinetics of fura-2 and azo-1 from temperture-jump relaxation measurement. Biophys J 1988;53:635–9.

Klingauf J, Neher E. Modeling buffered Ca^{2+} diffusion near the membrane: Implications for secretion in neuroendocrine cells. Biophys J 1997;72:674–90.

Lasser-Ross N, Miyakawa H, Lev-Ram W, Young SR, Ross WN. High time resolution fluorescence imaging with a CCD camera. J Neurosci Methods 1991;36:253–61.

Lim JS. Two Dimensional Signal and Image Processing. Englewood Cliffs, NJ: Prentice Hall, 1990:469–76.

Llinas R, Steinberg IZ, Walton K. Presynaptic calcium currents in squid giant synapse. Biophys J 1981;33:289–322.

Mammano F, Kros CJ, Ashmore JF. Patch clamped responses from outer hair cells in the intact adult organ of Corti. Pflüger's Arch 1995;430:745–50.

Markram H, Helm PJ, Sakmann B. Dendritic calcium transients evoked by single back-propagating action potentials in rat neocortical pyramidal neurons. J Physiol 1995;485:1–20.

McCobb DP, Beam KG. Action potential waveform voltage-clamp commands reveal striking differences in calcium entry via low and high voltage-activated calcium chanels. Neuron 1991;7:119–27.

Neher E. Correction for liquid junction potentials in patch clamp experiments. Methods Enzymol 1992;207:123–31.

Neher E, Augustine GJ. Calcium gradients and buffers in bovine chromaffin cells. J Physiol 1992;450:273–301.

Nowycky MC, Pinter MJ. Time courses of calcium and calcium-bound buffers following calcium influx in a model cell. Biophys J 1993;64:77–91.

Oppenheim AV, Shaffer RW. Discrete-Time Signal Processing. Englewood Cliffs, NJ: Prentice Hall, 1989:311–2.

Regehr WG, Atluri PP. Calcium transients in cerebellar granule cell presynaptic terminals. Biophys J 1995;68:2156–70.

Sala F, Hernández-Cruz A. Calcium diffusion modeling in a spherical neuron: relevance of buffering properties. Biophys J 1990;57:313–24.

Schaff J, Fink CC, Slepchenko B, Carson JH, Loew LM. Integrated framework for modeling and simulation of cell physiology with real image data: applications in calcium dynamics and electrophysiology. Biophys J 1997;73:1135–46.

Spruston N, Schiller Y, Stuart G, Sakmann B. Activity-dependent action potential invasion and calcium influx into hippocampal CA1 dendrites. Science 1995;268:297–300.

Stuart G, Spruston N, Sakmann B, Häusser M. Action potential initiation and backpropagation in neurons of the mammalian CNS. Trends Neurosci 1997;20:125–31.

Thomas AP, Delaville F. The use of fluorescent indicators for measurement of cytosolic-free calcium concentration in cell populations and single cells. In: McCormak JG, Cobbold PH, editors. Cellular Calcium. Oxford: IRL Press, 1988:1–54.

Tsubokawa H, Ross WN. IPSPs modulate spike backpropagation and associated $[Ca^{2+}]_i$ changes in the dendrites of hippocampal CA1 pyramidal neurons. J Neurophysiol 1996;76:2896–906.

Williams DA, Fogarty KE, Tsien RY, Fay FS. Calcium gradients in single smooth muscle cells revealed by the digital imaging microscope using Fura-2. Nature 1985;318:558–61.

Yamada WM, Koch C, Adams PR. Multiple channels and calcium dynamics. In: Koch C, Segev I, editors. Methods in Neuronal Modeling. Cambridge, MA: MIT Press, 1989:109–15.